






RESEARCH ARTICLE | APRIL 22 2024

Revisiting lattice thermal conductivity of CsCl: The crucial role of quartic anharmonicity

Xiaoying Wang; Minxuan Feng; Yi Xia; Jun Sun ; Xiangdong Ding ; Baowen Li ; Zhibin Gao  

 Check for updates

Appl. Phys. Lett. 124, 172201 (2024)

<https://doi.org/10.1063/5.0201393>



An innovative I-V characterization system for next-gen semiconductor R&D

Unique combination of ultra-low noise sourcing + high-sensitivity lock-in measuring capabilities

[Learn more](#)



Revisiting lattice thermal conductivity of CsCl: The crucial role of quartic anharmonicity

Cite as: Appl. Phys. Lett. **124**, 172201 (2024); doi: [10.1063/5.0201393](https://doi.org/10.1063/5.0201393)

Submitted: 30 January 2024 · Accepted: 2 April 2024 ·

Published Online: 22 April 2024



View Online



Export Citation



CrossMark

Xiaoying Wang,¹ Minxuan Feng,¹ Yi Xia,² Jun Sun,¹  Xiangdong Ding,¹  Baowen Li,^{3,4}  and Zhibin Gao^{1,a)} 

AFFILIATIONS

¹State Key Laboratory for Mechanical Behavior of Materials, School of Materials Science and Engineering, Xi'an Jiaotong University, Xi'an 710049, China

²Department of Mechanical and Materials Engineering, Portland State University, Portland, Oregon 97201, USA

³Department of Materials Science and Engineering, Department of Physics, Southern University of Science and Technology, Shenzhen, 518055, People's Republic of China

⁴International Quantum Academy, Shenzhen 518048, People's Republic of China

Note: This paper is part of the APL Special Collection on Advances in Thermal Phonon Engineering and Thermal Management.

^{a)}Author to whom correspondence should be addressed: zhibin.gao@xjtu.edu.cn

ABSTRACT

Thermal conductivity (κ_L) plays a critical role in thermal management applications. Usually, crystals with simpler structures exhibit higher κ_L due to fewer phonon scatterings. However, cesium chloride (CsCl) presents an anomaly, demonstrating an unexpectedly low κ_L of $1.0 \text{ W m}^{-1} \text{ K}^{-1}$ at 300 K, as observed in Professor Iversen's experimental measurement despite its simple structure. This prompts a need for understanding anomalous low κ_L and matching theory with experimental observations. Our study brings forth several findings for CsCl: (i) relying solely on three-phonon scattering inadequately captures κ_L . (ii) Anharmonic phonon renormalization significantly contributes to increased κ_L . (iii) Coherent phonons align temperature-dependent κ_L closely with the experiment. This work not only enhances understanding of anomalous κ_L in CsCl but also provides an approach to bridge the gap between experiment and theory in other crystals.

Published under an exclusive license by AIP Publishing. <https://doi.org/10.1063/5.0201393>

Tracing the roots of extreme semiconductor thermal conductivity is an undertaking fraught with challenges. Materials with intrinsically low thermal conductivity are of significance in technological applications such as thermal management in heat-insulating coatings,^{1,2} thermal barrier coatings,^{3,4} and thermoelectric (TE) devices^{5,6} for waste heat recovery. Therefore, a fundamental understanding of the microscopic mechanisms of heat transport in low lattice thermal conductivity (κ_L) and related materials is very beneficial in exploring the complex nature of material physics^{7,8} and designing efficient thermal management devices.²

Cesium halides CsX (X = Cl, Br, I) are renowned for their photoelectric properties and large dielectric constants, rendering them promising candidates for applications in optical devices^{9,10} and photoelectric fields.¹¹ Cesium chloride (CsCl), for instance, finds application as a scintillation crystal in electromagnetic calorimeters and positron emission tomography.^{12–14}

CsCl, with its simple AB-type cubic crystal structure, has drawn attention due to unexpected findings in its ultralow κ_L . Typically, low κ_L is associated with factors such as large atomic mass, complex crystal

structures, and loosely bonded atoms.^{15–17} However, CsCl has simple crystal structure, raising questions about anomalous κ_L . Despite its crystalline nature and only two atoms in the primitive cell,^{18,19} experimental results indicate an unusually low thermal conductivity of CsCl at room temperature, measuring only $1.0 \text{ W m}^{-1} \text{ K}^{-1}$.²⁰ This value is even lower than that of single-crystal Bi_2Te_3 nanowires, which records $1.47 \text{ W m}^{-1} \text{ K}^{-1}$ at 300 K.²¹

For κ_L of CsCl, in comparison with experimental measurements, there appears to be a significant mismatch of thermal conductivity between experimental and theoretical calculations,²² with an underestimation of the optical phonon modes, especially near the zone center.¹⁹ This discrepancy is evident in the latest experimental measurements, which remain largely unexplored and pose an open question.²⁰ We speculate that this discrepancy may stem from overlooking self-consistent phonons, high-order phonon scattering, coherent phonons, and variations in lattice constants.

To minimize the gap between the theory and the experiment, an *ab initio* calculation performed by VASP²³ based on the Boltzmann transport equation²⁴ is an effective way to calculate thermal transport

phenomena in CsCl. We consider more accurate quartic anharmonicity, concluding higher-order interatomic interactions^{25–30} and temperature renormalization.^{31,32} In addition, conventional κ_L calculations, rooted in the Peierls–Boltzmann transport equation, tend to overlook the off diagonal term in the heat flux operator of the Wigner distribution element. This oversight also may create a gap between theoretical predictions and experimental measurements.^{7,8,33–37}

CsCl crystallizes in the cubic structure (space group $\text{pm}\bar{3}\text{m}$ [221]) as depicted in Fig. 1(a), where Cs and Cl occupy the 1a and 1b sites, totaling two atoms in the primitive cell, as shown in the top right sketch of Fig. 1(a). Based on the three-phonon (3ph) scattering, we calculate κ_L for CsCl in the temperature range from 50 to 300 K, shown in the brown line in Fig. 1(b). Interestingly, there exists a gap between this result from the 3ph calculation and the experiment in black five-pointed stars²⁰ and purple cubes.³⁸ Note that we use the full iterative solution to Boltzmann transport equation³⁹ instead of bare relaxation time approximation (RTA) in the previous work.¹⁹ In addition, our optimized lattice constant from the local-density approximation (LDA) is 3.974 Å rather than the 4.039 Å in their report. More lattice constant details are shown in the supplementary material Table I.

In comparison with harmonic approximation (HA) considering 3ph scattering (HA + 3ph), κ_L based on HA + 3,4ph decreases due to the additional four-phonon (4ph) scattering. Furthermore, the gap between the 3ph and 4ph denoted as $\Delta\kappa$ ($\Delta\kappa = \kappa_{HA}^{3ph} - \kappa_{HA}^{3,4ph}$) increases with temperature. This can be attributed to the fact that the scattering rate of the 4ph (τ_4^{-1}) is inversely proportional to the square of the temperature T^2 , whereas only the scattering rate of the 3ph (τ_3^{-1}) is inversely proportional to the temperature T .^{40–42} Consequently, 4ph is more strongly affected as the temperature increases. Nevertheless, the thermal conductivity of $\kappa_{HA}^{3,4ph}$ is significantly lower than the experimental result.²⁰

As shown in Fig. 1(b), when compared to HA + 3ph, the thermal conductivity of SCPH + 3ph (κ_p^{3ph} in green triangle solid line) increases significantly. This notable change is primarily attributed to

the temperature effect. Consequently, the anharmonic phonon renormalization (APRN) effect tends to enhance κ_L of CsCl at various temperatures.³⁵ However, we find that the slope of the temperature-dependent κ_L curve of κ_p^{3ph} is a slightly different from the experiment. Therefore, we further calculate coherent phonon contribution (κ_c), represented by the green diamond solid line in Fig. 1(b). We find the absolute value of κ_c only contributes 5% to κ_L , but it changes the slope of the curve, resulting in the final κ_L alignment well with the experiment.²⁰

Based on the general relationship of the power law between the thermal conductivity and the temperature $\kappa \propto \frac{1}{T^\alpha}$, we fit the computational temperature-dependent lattice thermal conductivity. In the theory, α is somewhere between 0 and 2, reflecting the competition between scattering processes generated by the phonon–phonon scattering such as the cubic and quartic anharmonic terms.⁸ In comparison with $\kappa_{HA}^{3ph} \propto T^{-0.81}$, $\kappa_{HA}^{3,4ph} \propto T^{-0.88}$, $\kappa_p^{3ph} \propto T^{-0.59}$, and $\kappa_p^{3,4ph} \propto T^{-1.04}$, considering κ_c of $\kappa_p^{3,4ph} + \kappa_c \propto T^{-1.01}$ relatively aligns with the latest experimental value $T^{-1.01}$.²⁰ Typically, the contribution of coherent phonons from the coherent Wigner distributions is relatively large only in complex materials.^{7,43}

We were pleasantly surprised, for simple crystals, even if the absolute value of κ_c from coherent phonons is much smaller than κ_p from the population phonons, κ_c will change the relationship of slope between κ_L and the temperature. Therefore, κ_c contributes a vital role in the strong phonon anharmonicity of CsCl.

We illustrate the atomic displacement parameter (ADP), representing the mean square displacement of an atom about its equilibrium position in CsCl, at different temperatures in Fig. 2(a). Cs and Cl exhibit similar displacement curves with a large isotropic, especially at low temperatures, where they almost overlap, with a slight separation occurring at 150 K as the temperature increases. This observation aligns well with experimental measurement.²⁰ Both Cs and Cl atoms exhibit a large thermal vibration (ADP ≈ 0.025 Å² at 300 K) with displacement predominantly along the c -axis. Notably, the interatomic

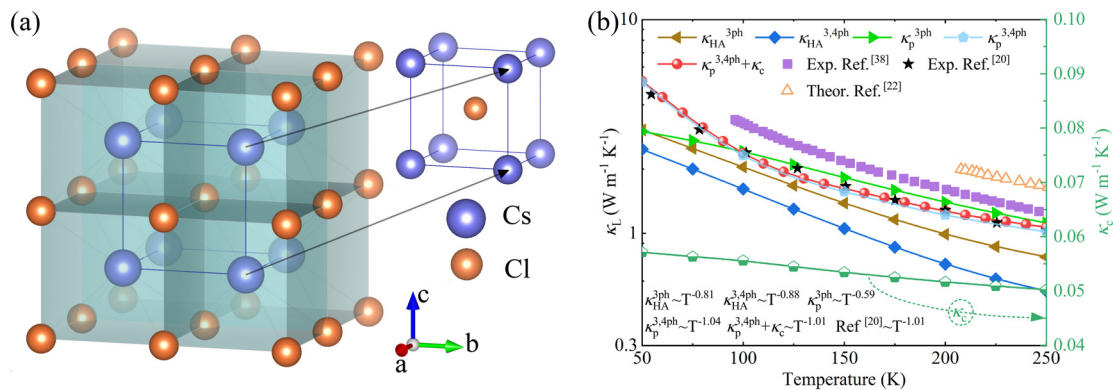


FIG. 1. (a) The crystal structure of body-centered cubic CsCl, with the primitive cell at the top right containing two atoms represented by purple (Cs) and orange (Cl) colors. (b) κ_L for CsCl with various scenarios. " κ_{HA}^{3ph} " represents the harmonic approximation (HA) considering three-phonon (3ph) interactions. " $\kappa_{HA}^{3,4ph}$ " illustrates harmonic approximation containing both three-phonon (3ph) and four-phonon (4ph) interactions. " κ_p^{3ph} " denotes the self-consistent phonon (SCPH) theory considering 3ph interactions. " $\kappa_p^{3,4ph}$ " stands for SCPH, 3ph, and 4ph scatterings. " κ_c " represents the thermal conductivity of off diagonal terms. The black five-pointed stars and purple squares both represent the experiment data in 2017 Reproduced with permission from Sist *et al.*, *Angew. Chem. Int. Ed.* **129**, 3679–3683 (2017). Copyright 2017 German Chemical Society²⁰ and 1982 Reproduced with permission from Gerlich and Andersson, *J. Phys. C: Solid State Phys.* **15**, 5211 (1982). Copyright 1982 IOP Science,³⁸ while orange hollow triangles represent the theoretical data from first-principles calculations only considering 3ph scattering Reproduced with permission from Li *et al.*, *Phys. Chem. Chem. Phys.* **24**, 29961–29965 (2022). Copyright 2022 Royal Society of Chemistry.²²

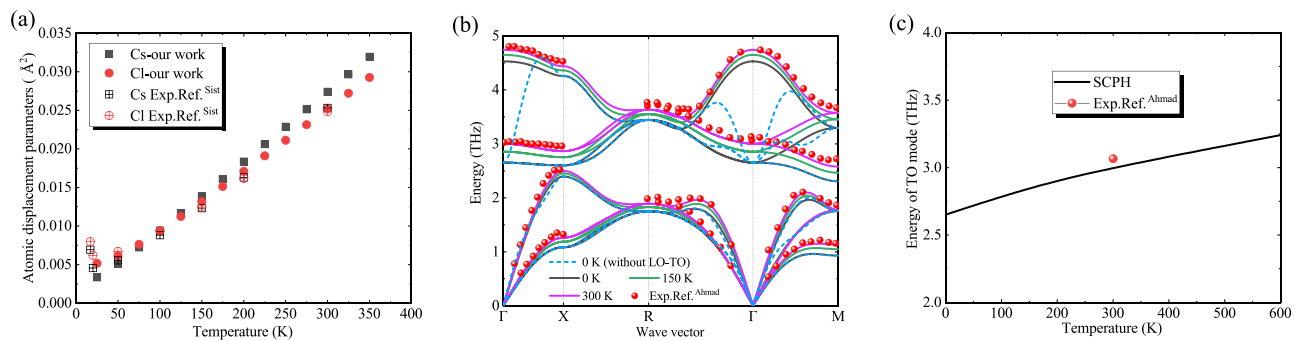


FIG. 2. (a) The atomic displacement parameters (ADP) of Cs and Cl in the direction of the z-axis (0 0 1). Solid dots and cubes represent the data we calculated, while the hollow points are experimental data. Reproduced with permission from Sist *et al.*, *Angew. Chem. Int. Ed.* **129**, 3679–3683 (2017). Copyright 2017 German Chemical Society.²⁰ (b) Phonon dispersions of CsCl with/without the longitudinal optical-transversal optical (LO-TO) splitting at 0, 150, and 300 K, respectively. The red points describe the experimental outcomes from the reference. Reproduced with permission from Ahmad *et al.*, *Phys. Rev. B* **6**, 3956 (1972). Copyright 1972 AIP Publishing LLC.¹⁸ (c) The calculated temperature-dependent energy of zone-center transversal optical (TO) mode compared with the SCPH method at various temperatures and experiment. Reproduced with permission from Ahmad *et al.*, *Phys. Rev. B* **6**, 3956 (1972). Copyright 1972 AIP Publishing LLC.¹⁸

distance of Cs and Cl is significantly influenced by temperature. Extrapolating for the CsCl system, it is crucial to consider the impact of temperature on κ_L . We calculate this temperature effect using the self-consistent phonon theory.^{26,28–30}

The significance of longitudinal optical-transversal optical (LO-TO) splitting by harmonic approximation phonon dispersion is depicted in Fig. 2(b). To provide a clearer understanding of the effect of APRN, we present the calculated phonon dispersion considering LO-TO phonon splitting from 0 to 300 K, compared with experimental data.¹⁵ By employing the density functional perturbation theory, we obtain Born effective charges and dielectric tensors for CsCl, resulting in $Z^*(\text{Cs}) = Z^*(\text{Cl}) = 1.33$, $\epsilon = 3.00$.

Subsequently, we conduct a thermodynamic analysis of the temperature impact on the phonon spectrum at various temperatures, as depicted in Fig. 2(b). The illustration shows that both the acoustic and optical phonon branches experience stiffening as the temperature rises from 0 to 300 K. As the temperature increases, there is a noteworthy enhancement in the frequency of the phonon dispersion, particularly observed at the Γ point within the transversal optical branch around 3 THz. This enhancement is a result of considering anharmonic phonon renormalization. The phonon dispersion aligns well with experimental results,²⁰ emphasizing the significance of APRN and LO-TO splitting in the CsCl.

According to Fig. 2(c), the energy linked to the primary peak of the zone-center TO mode demonstrates variation with temperature. It is noteworthy that APRN effectively reproduces the energy of the zone-center TO mode across different temperatures.¹⁸ A notable outcome of our investigation is the ability to accurately capture the temperature dependence of the zone-center TO mode, achieved by considering quartic anharmonicity.

To elucidate the physical mechanisms behind the ultralow thermal conductivity and anharmonicity of CsCl, Fig. 3(a) presents the cumulative lattice thermal conductivity and frequency-resolved cumulative κ_L plotted against phonon frequency across different calculation methods. According to frequency-resolved cumulative κ_L , in the frequency around 1 THz, all three models show a maximum value. It means that the phonons vibrate most vigorously and intensively around this frequency. The acoustic

phonon frequency ($\text{Fre} = 1$ THz) is considered representative of the frequency of dominating heat-carrying phonons in bulk CsCl crystal at 300 K. Figure 3(b) shows the phase space of phonon scattering, and Fig. 3(c) is the total scattering rates of 3ph and 4ph, taking into account temperature effects at 300 K. Across the 1 THz range, it becomes evident that 4ph and temperature effects significantly influence heat transport for the CsCl material.

Phase space refers to the availability of phonon–phonon scattering channels. The strength of scattering in each accessible channel determines the phonon relaxation time, further influencing κ_L . As shown in Fig. 3(b), the phase space of 3ph surrounding 1 THz is larger than other frequencies, and the phase space of 4ph near 1 THz is roughly equivalent to other frequencies. However, in terms of phase space, SCPH does not appear to have a significant impact. Therefore, the scattering channels of 4ph are essential to heat transport, and κ_L is smaller than when considering only 3ph scattering. Consequently, it is considered that 4ph increases the scattering phase space, thus enhancing the phonon scattering.

Scattering rates are depicted in Fig. 3(c). Scattering rates of 3ph (SR_{3ph}) show a slightly more significant impact than 4ph (SR_{4ph}), $\text{SR}_{3ph} \geq \text{SR}_{4ph}$, but it is undeniable that 4ph plays a significant role as well. Therefore, by including 4ph scattering, κ_L is generally smaller than when considering only 3ph scattering, resulting in lower κ_L with increasing temperature, shown in Fig. 1(b). However, the temperature-dependent APRN reduces the scattering rates, leading to a slight rise in κ_L . Figure 3(d) demonstrates the temperature effect on ν^2 . We observe a distinct frequency shift, an increase in ν originating from the temperature effect, as declared by the renormalized phonon dispersions in Fig. 2(b).

We evaluate the 3ph scattering channels involving three acoustic phonons (AAA), two acoustic phonons combining with one optical phonon (AAO), and one acoustic phonon combining with two optical phonons (AOO), as shown in Fig. 4(a). The scattering process of the AAO mode is found to be much stronger than others at frequencies below 2 THz, meaning the entanglement in AAO phonons plays a dominant role in heat transport. However, spanning the range from 2 THz to 5 THz of the optical phonons, the AOO mode is the major scattering channel.

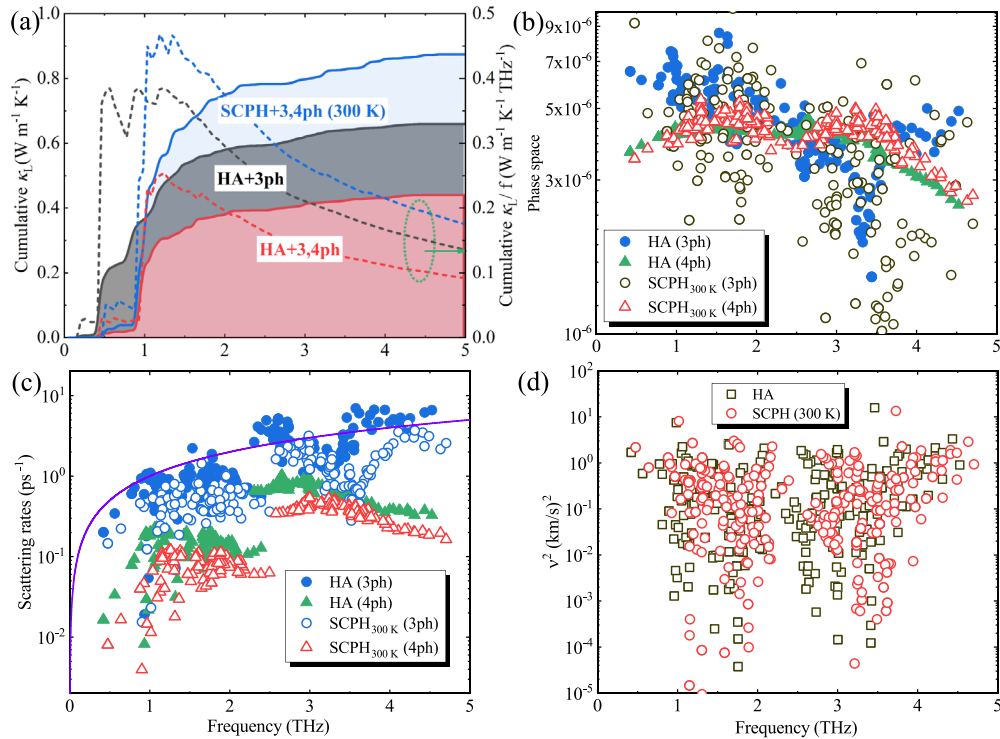


FIG. 3. (a) Cumulative κ_L and frequency-resolved cumulative κ_L computed at different levels of approximation [see legend in Fig. 1(b)] with frequency at 300 K. The blue, black, and red lines represent SCPH + 3,4ph, HA + 3ph, and HA + 3,4ph, respectively. (b) Investigation of the influence of phonon scattering phase space in SCPH effect, 3ph, and 4ph at 300 K. The blue, green, black, and red points represent HA + 3ph, HA + 4ph, SCPH + 3ph, and SCPH + 4ph, respectively. (c) Phonon-phonon scattering rates by comparing SCPH effect, 3ph, and 4ph at 300 K with the same color meaning as (b). The solid purple lines in (c) indicate the Ioffe-Regel limit in time ($1/\tau = \omega/2\pi$).³⁴ (d) The square of the phonon group velocity v^2 in the harmonic approximation (black cubes) and self-consistent phonon renormalization methods (red circles) at 300 K.

The calculated total Grüneisen parameter (γ) is 2.40 for CsCl, as illustrated in Fig. 4(b), indicating more anharmonicity compared to 0.73, 0.78, and 1.93 for GeSe, SnSe, and PbSe with the same crystal symmetry.⁴⁴ We calculate γ for various phonon branches to evaluate

the anharmonicity of CsCl. In the frequency-dominant heat transport range of 1 THz, γ is primarily affected by the transverse acoustic (TA) modes, which exhibit large phonon vibrations and stronger heat transport operators.

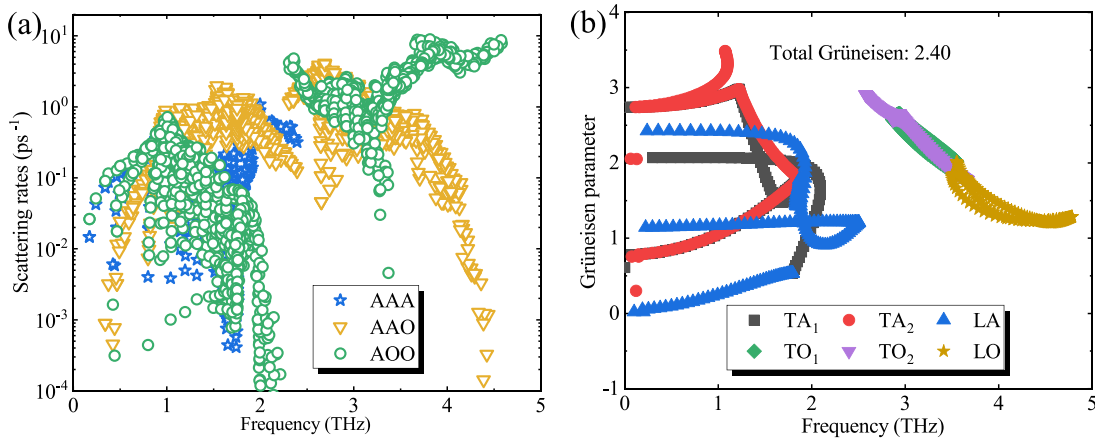


FIG. 4. (a) Calculated three-phonon scattering rates for different scattering channels (AAA, AAO, and AOO) at 300 K. A and O stand for the acoustic and optical phonons. (b) The Grüneisen parameter for various phonon modes [transversal acoustic (TA), longitudinal acoustic (LA), transversal optical (TO), and longitudinal optical (LO)] at 300 K. The total Grüneisen parameter of CsCl is 2.40.

22 April 2024 11:36:40

In summary, the anharmonicity ($\gamma=2.40$) of CsCl is strong entanglement in AAO phonons and obvious four-phonon scattering. Our study reveals that 4ph scattering, phonon renormalization, and the off diagonal terms of the heat flux operators cannot be neglected, even in the simple body-centered cubic crystal. Particularly, we made an unexpected discovery in simple crystals, although the absolute value of the lattice thermal conductivity corresponding to coherent phonons is small, it corrects the function relationship between thermal conductivity and temperature, thus being mildly consistent with the experimental measurement results.

See the supplementary material for the details of the calculation method, comparison of lattice constants, functionals, and lattice thermal conductivity from computational and experimental references for CsCl.

The work is sponsored by the Key Research and Development Program of the Ministry of Science and Technology under Grant No.2023YFB4604100. We acknowledge the support of the National Natural Science Foundation of China (Nos. 12104356 and 52250191), China Postdoctoral Science Foundation (No. 2022M712552), the Opening Project of Shanghai Key Laboratory of Special Artificial Microstructure Materials and Technology (No. Ammt2022B-1), and the Fundamental Research Funds for the Central Universities. We also acknowledge the support by HPC Platform, Xi'an Jiaotong University.

AUTHOR DECLARATIONS

Conflict of Interest

The authors have no conflicts to disclose.

Author Contributions

Xiaoying Wang and Minxuan Feng contributed equally to this work.

Xiaoying Wang: Investigation (equal); Methodology (equal); Resources (equal); Software (equal); Writing – original draft (equal). **Minxuan Feng:** Investigation (equal); Software (equal). **Yi Xia:** Supervision (equal); Writing – review & editing (equal). **Jun Sun:** Supervision (equal). **Xiangdong Ding:** Supervision (equal). **Baowen Li:** Supervision (equal). **Zhibin Gao:** Visualization (equal); Writing – original draft (equal); Writing – review & editing (equal).

DATA AVAILABILITY

The data that support the findings of this study are available from the corresponding author upon reasonable request.

REFERENCES

- Q. D. Gibson, T. Zhao, L. M. Daniels, H. C. Walker, R. Daou, S. Hébert, M. Zanella, M. S. Dyer, J. B. Claridge, B. Slater, M. W. Gaultois, F. Corà, J. Alaria, and M. J. Rosseinsky, "Low thermal conductivity in a modular inorganic material with bonding anisotropy and mismatch," *Science* **373**, 1017–1022 (2021).
- X. Qian, J. Zhou, and G. Chen, "Phonon-engineered extreme thermal conductivity materials," *Nat. Mater.* **20**, 1188–1202 (2021).
- D. R. Clarke and S. R. Phillpot, "Thermal barrier coating materials," *Mater. Today* **8**, 22–29 (2005).

- B. Liu, Y. Liu, C. Zhu, H. Xiang, H. Chen, L. Sun, Y. Gao, and Y. Zhou, "Advances on strategies for searching for next generation thermal barrier coating materials," *J. Mater. Sci. Technol.* **35**, 833–851 (2019).
- L.-D. Zhao, S.-H. Lo, Y. Zhang, H. Sun, G. Tan, C. Uher, C. Wolverton, V. P. Dravid, and M. G. Kanatzidis, "Ultralow thermal conductivity and high thermoelectric figure of merit in SnSe crystals," *Nature* **508**, 373–377 (2014).
- W. G. Zeier, A. Zevalkink, Z. M. Gibbs, G. Hautier, M. G. Kanatzidis, and G. J. Snyder, "Thinking like a chemist: Intuition in thermoelectric materials," *Angew. Chem. Int. Ed.* **55**, 6826–6841 (2016).
- M. Simoncelli, N. Marzari, and F. Mauri, "Unified theory of thermal transport in crystals and glasses," *Nat. Phys.* **15**, 809–813 (2019).
- X. Wang, Z. Gao, G. Zhu, J. Ren, L. Hu, J. Sun, X. Ding, Y. Xia, and B. Li, "Role of high-order anharmonicity and off-diagonal terms in thermal conductivity: A case study of multiphase CsPbBr₃," *Phys. Rev. B* **107**, 214308 (2023).
- P. Masselin, D. Le Coq, L. Calvez, E. Petracovschi, E. Lépine, E. Bychkov, and X. Zhang, "CsCl effect on the optical properties of the 80GeS₂–20Ga₂S₃ base glass," *Appl. Phys. A* **106**, 697–702 (2012).
- G. Yoshikawa, M. Kiguchi, K. Ueno, A. Koma, and K. Saiki, "Visible light photoemission and negative electron affinity of single-crystalline CsCl thin films," *Surf. Sci.* **544**, 220–226 (2003).
- A. Soler and F. R. Sánchez, "F-centre photoelectric materials as image storage targets," *Phys. Status Solidi A* **11**, 67–74 (1972).
- C.-J. Lee, J.-I. Han, D.-K. Choi, and D.-G. Moon, "Transparent organic light-emitting devices with CsCl capping layers on semitransparent Ca/Ag cathodes," *Mater. Sci. Eng. B* **172**, 76–79 (2010).
- V. S. Shevelev, A. V. Ishchenko, A. S. Vanetsev, V. Nagirnyi, and S. I. Omelkov, "Ultrafast hybrid nanocomposite scintillators: A review," *J. Lumin.* **242**, 118534 (2022).
- M. Nikl, "Wide band gap scintillation materials: Progress in the technology and material understanding," *Phys. Status Solidi A* **178**, 595–620 (2000).
- Y. Luo, X. Yang, T. Feng, J. Wang, and X. Ruan, "Vibrational hierarchy leads to dual-phonon transport in low thermal conductivity crystals," *Nat. Commun.* **11**, 2554 (2020).
- M. Wu, Enamullah, and L. Huang, "Unusual lattice thermal conductivity in the simple crystalline compounds TLXTe₂ (X = Ga, In)," *Phys. Rev. B* **100**, 075207 (2019).
- J. Li, W. Hu, and J. Yang, "High-throughput screening of rattling-induced ultralow lattice thermal conductivity in semiconductors," *J. Am. Chem. Soc.* **144**, 4448–4456 (2022a).
- A. A. Z. Ahmad, H. G. Smith, N. Wakabayashi, and M. K. Wilkinson, "Lattice dynamics of cesium chloride," *Phys. Rev. B* **6**, 3956 (1972).
- C. He, C.-E. Hu, T. Zhang, Y.-Y. Qi, and X.-R. Chen, "Lattice dynamics and thermal conductivity of cesium chloride via first-principles investigation," *Solid State Commun.* **254**, 31–36 (2017).
- M. Sist, K. F. F. Fischer, H. Kasai, and B. B. Iversen, "Low-temperature anharmonicity in cesium chloride (CsCl)," *Angew. Chem. Int. Ed.* **129**, 3679–3683 (2017).
- D. Park, S. Park, K. Jeong, H.-S. Jeong, J. Y. Song, and M.-H. Cho, "Thermal and electrical conduction of single-crystal Bi₂Te₃ nanostructures grown using a one step process," *Sci. Rep.* **6**, 19132 (2016).
- S. Li, Z. Zeng, Y. Pu, and Y. Chen, "Pressure effects on the anomalous thermal transport and anharmonic lattice dynamics of CsX (X = Cl, Br, and I)," *Phys. Chem. Chem. Phys.* **24**, 29961–29965 (2022b).
- G. Kresse and J. Furthmüller, "Efficient iterative schemes for *ab initio* total-energy calculations using a plane-wave basis set," *Phys. Rev. B* **54**, 11169–11186 (1996).
- R. E. Peierls and L. D. Roberts, "Quantum theory of solids," *Phys. Today* **9**(5), 29 (1956).
- N. R. Werthamer, "Self-consistent phonon formulation of anharmonic lattice dynamics," *Phys. Rev. B* **1**, 572 (1970).
- T. Tadano and S. Tsuneyuki, "Self-consistent phonon calculations of lattice dynamical properties in cubic SrTiO₃ with first-principles anharmonic force constants," *Phys. Rev. B* **92**, 054301 (2015).
- T. Feng and X. Ruan, "Quantum mechanical prediction of four-phonon scattering rates and reduced thermal conductivity of solids," *Phys. Rev. B* **93**, 045202 (2016).
- F. Zhou, W. Nielson, Y. Xia, and V. Ozoliņš, "Lattice anharmonicity and thermal conductivity from compressive sensing of first-principles calculations," *Phys. Rev. Lett.* **113**, 185501 (2014).

- ²⁹F. Zhou, W. Nielson, Y. Xia, and V. Ozoliņš, “Compressive sensing lattice dynamics. I. General formalism,” *Phys. Rev. B* **100**, 184308 (2019).
- ³⁰F. Zhou, B. Sadigh, D. Åberg, Y. Xia, and V. Ozoliņš, “Compressive sensing lattice dynamics. II. Efficient phonon calculations and long-range interactions,” *Phys. Rev. B* **100**, 184309 (2019).
- ³¹X. Yang, T. Feng, J. Li, and X. Ruan, “Stronger role of four-phonon scattering than three-phonon scattering in thermal conductivity of III-V semiconductors at room temperature,” *Phys. Rev. B* **100**, 245203 (2019).
- ³²L. Lindsay, D. A. Broido, and T. L. Reinecke, “First-principles determination of ultrahigh thermal conductivity of boron arsenide: A competitor for diamond?,” *Phys. Rev. Lett.* **111**, 025901 (2013).
- ³³Z. Tong, A. Pecchia, C. Yam, T. Dumitrica, and T. Frauenheim, “Glass-like transport dominates ultralow lattice thermal conductivity in modular crystalline $\text{Bi}_4\text{O}_4\text{SeCl}_2$,” *Nano Lett.* **23**, 9468–9473 (2023).
- ³⁴M. Simoncelli, N. Marzari, and F. Mauri, “Wigner formulation of thermal transport in solids,” *Phys. Rev. X* **12**, 041011 (2022).
- ³⁵Y. Xia, V. I. Hegde, K. Pal, X. Hua, D. Gaines, S. Patel, J. He, M. Aykol, and C. Wolverton, “High-throughput study of lattice thermal conductivity in binary rocksalt and zinc blende compounds including higher-order anharmonicity,” *Phys. Rev. X* **10**, 041029 (2020).
- ³⁶Y. Xia, V. Ozoliņš, and C. Wolverton, “Microscopic mechanisms of glasslike lattice thermal transport in cubic $\text{Cu}_{12}\text{Sb}_4\text{S}_{13}$ tetrahedrites,” *Phys. Rev. Lett.* **125**, 085901 (2020).
- ³⁷J. Chen, J. He, D. Pan, X. Wang, N. Yang, J. Zhu, S. A. Yang, and G. Zhang, “Emerging theory and phenomena in thermal conduction: A selective review,” *Sci. China Phys. Mech. Astron.* **65**, 117002 (2022).
- ³⁸D. Gerlich and P. Andersson, “Temperature and pressure effects on the thermal conductivity and heat capacity of CsCl, CsBr and CsI,” *J. Phys. C: Solid State Phys.* **15**, 5211 (1982).
- ³⁹W. Li, J. Carrete, N. A. Katcho, and N. Mingo, “ShengBTE: A solver of the Boltzmann transport equation for phonons,” *Comput. Phys. Commun.* **185**, 1747–1758 (2014).
- ⁴⁰S. I. Kim, K. H. Lee, H. A. Mun, H. S. Kim, S. W. Hwang, J. W. Roh, D. J. Yang, W. H. Shin, X. S. Li, Y. H. Lee, G. J. Snyder, and S. W. Kim, “Dense dislocation arrays embedded in grain boundaries for high-performance bulk thermoelectrics,” *Science* **348**, 109–114 (2015).
- ⁴¹M. Hong, T. C. Chasapis, Z.-G. Chen, L. Yang, M. G. Kanatzidis, G. J. Snyder, and J. Zou, “n-type $\text{Bi}_2\text{Te}_{3-x}\text{Se}_x$ nanoplates with enhanced thermoelectric efficiency driven by wide-frequency phonon scatterings and synergistic carrier scatterings,” *ACS Nano* **10**, 4719–4727 (2016).
- ⁴²T. Feng, L. Lindsay, and X. Ruan, “Four-phonon scattering significantly reduces intrinsic thermal conductivity of solids,” *Phys. Rev. B* **96**, 161201 (2017).
- ⁴³L. Isaeva, G. Barbalinardo, D. Donadio, and S. Baroni, “Modeling heat transport in crystals and glasses from a unified lattice-dynamical approach,” *Nat. Commun.* **10**, 3853 (2019).
- ⁴⁴P.-F. Liu, T. Bo, J. Xu, W. Yin, J. Zhang, F. Wang, O. Eriksson, and B.-T. Wang, “First-principles calculations of the ultralow thermal conductivity in two-dimensional group-IV selenides,” *Phys. Rev. B* **98**, 235426 (2018).